Published in final edited form as:
Cancer Res. 2008 October 15; 68(20): 8369–8376. doi:10.1158/0008-5472.CAN-08-1771.

Early Therapy Evaluation of Combined Anti-DR5 Antibody and Gemcitabine in Orthotopic Pancreatic Tumor Xenografts by Diffusion Weighted Magnetic Resonance Imaging

Hyunki Kim[1,2,7,8], **Desiree E. Morgan**[1,7], **Donald J. Buchsbaum**[3,7], **Huadong Zeng**[4,7], **William E. Grizzle**[5], **Jason M. Warram**[5], **Cecil R. Stockard**[7], **Lacey R. McNally**[1,3], **Joshua W. Long**[6], **Jeffrey C. Sellers**[3], **Andres Forero**[4,7], and **Kurt R. Zinn**[1,4,5,7,8]

1 *Department of Radiology, University of Alabama at Birmingham, Birmingham, Alabama 35294*

2 *Department of Biomedical Engineering, University of Alabama at Birmingham, Birmingham, Alabama 35294*

3 *Department of Radiation Oncology, University of Alabama at Birmingham, Birmingham, Alabama 35294*

4 *Department of Medicine, University of Alabama at Birmingham, Birmingham, Alabama 35294*

5 *Department of Pathology, University of Alabama at Birmingham, Birmingham, Alabama 35294*

6 *Department of Surgery, University of Alabama at Birmingham, Birmingham, Alabama 35294*

7 *Comprehensive Cancer Center, University of Alabama at Birmingham, Birmingham, Alabama 35294*

Abstract

Early therapeutic efficacy of anti-DR5 antibody (TRA-8) combined with gemcitabine was measured using diffusion-weighted magnetic resonance imaging (DWI) in an orthotopic pancreatic tumor model. Groups 1–4 of SCID mice (n=5–7/group) bearing orthotopically implanted, luciferase-positive human pancreatic tumors (MIA PaCa-2) were subsequently (4–5 weeks thereafter) injected with saline (control), gemcitabine (120mg/kg), TRA-8 (200μg), or TRA-8 combined with gemcitabine, respectively, on day 0. DWI, anatomical MRI, and bioluminescence imaging were performed on days 0, 1, 2, and 3 after treatment. Three tumors from each group were collected randomly on day 3 after imaging, and TUNEL staining was performed to quantify apoptotic cellularity. At just 1 day after starting therapy, the changes of apparent diffusion coefficient (ADC) in tumor regions for groups 3 (TRA-8) and 4 (TRA-8/Gem) were 21±9% (mean±SE) and 27±3%, respectively, significantly higher ($p < 0.05$) than those of groups 1 (−1±5%) and 2 (−2±4%). There was no statistical difference in tumor volumes for the groups at this time. The mean ADC values of groups 2–4 gradually increased over 3 days, which were concurrent with tumor-volume regressions and bioluminescence-signal decreases. Apoptotic-cell densities of tumors in groups 1–4 were 0.7 ±0.4%, 0.6±0.2%, 3.1±0.9%, and 4.7±1.0%, respectively, linearly proportional to the ADC changes on day 1. Further, the ADC changes were highly correlated with the previously reported mean survival times of animals treated with the same agents and doses. This study supports the clinical use of DWI for pancreatic tumor patients for early assessment of drug efficacy.

8Requests for reprints: Hyunki Kim (E-mail: Hyunki@uab.edu), BDB 815, University of Alabama at Birmingham, Birmingham, AL, 35294-0012, or Kurt R. Zinn (E-mail: Kurtzinn@uab.edu), BDB 802, University of Alabama at Birmingham, Birmingham, AL, 35294-0012.

Dr. Buchsbaum has intellectual property interest related to TRA-8.

Presentation from the American Cancer Society (Cancer Statistics, 2007)

Keywords

DR5; TRA-8; pancreatic cancer; DWI; apoptosis

Introduction

Pancreatic cancer has highest fatality rate of all cancers and is the fourth leading cause of cancer death in the United States in 2007* The efficacies of current drugs such as 5-FU, irinotecan, oxaliplatin, and gemcitabine are modest in most pancreatic-cancer patients (1-5). A therapeutic approach that selectively kills pancreatic cancer would be highly advantageous, and may be possible by targeting death receptors expressed on pancreatic tumor cells (6,7). TRAIL (Tumor necrosis factor-Related Apoptosis-Inducing Ligand) induces apoptosis in most tumor cell lines (8–11), via death receptor-4 (DR4) and death receptor-5 (DR5) (12–15). Of concern, the significant cytotoxicity of TRAIL in human hepatocytes may limit its clinical application (16). The hepatoxicity of TRAIL may be related to binding to multiple receptors (17–20); the limitation could be overcome by using an agonistic antibody targeting only one death receptor.

A novel murine, monomeric monoclonal antibody (TRA-8) was developed specifically to target DR5, predominantly expressed in most cancer cells, but not in normal cells (21). The anti-tumor efficacy of TRA-8 in five pancreatic-cancer cell lines has been measured using *in vitro* cytotoxicity assay; each cell line had a unique sensitivity for TRA-8 (22). Pancreatic tumor cell resistance might be reduced by exposure to additional drugs and/or radiation, which destabilizes the mitochondrial membrane and subsequently releases cytochrome c, leading to the activation of caspase 3 (23,24). Although combination therapy might be superior to monotherapy, a certain range of therapeutic efficacy is predicted in patients with genetically heterogeneous tumors. Therefore it would be ideal to determine the degree of tumor response in each individual patient following treatment, and then to adjust therapeutic strategy at the earliest possible time in efforts to improve survival.

Diffusion-weighted magnetic resonance imaging (DWI) has been successfully applied in various cancers to evaluate early response against effective therapy (25–27), and has been positively correlated with eventual clinical outcome (28). In the early stage of apoptosis, water in the extra-cellular space is increased due to apoptotic volume decrease (AVD). This quantitative change in water can be measured as the apparent diffusion coefficient (ADC), depicted on DWI with high sensitivity, prior to visible change of tumor morphology and size. Early assessment of response should enable application of appropriate agents during neoadjuvant chemotherapy. Effective neoadjuvant chemotherapy will result in a decrease of primary tumor size to facilitate surgical tumor removal as well as prevent potential metastasis.

The aim of this study was to develop a DWI protocol to detect early therapeutic response following treatment with TRA-8 combined with gemcitabine in a mouse model of orthotopic pancreatic tumor, and to correlate the early ADC change with animal survival time. In addition, living tumor mass was monitored by bioluminescence imaging to confirm the killing efficacy by the combined therapy, while simultaneously the tumor volumes were measured using standard anatomical MRI; both parameters were compared with the ADC values from repeated DWI. The results show that noninvasive imaging parameters developed in this study accurately reflected the efficacy of the novel combined therapy in pancreatic cancer, and thus may be readily translated to a clinical trial.

Materials and Methods

Reagents and cell lines

All reagents were from Fisher (Pittsburgh, PA) unless otherwise specified. Human pancreatic cell line, MIA PaCa-2, was a gift from Dr. M. Hollingsworth (University of Nebraska). MIA PaCa-2 cells were cultured in DMEM (Mediatech Inc, Herndon VA) with 10% fetal bovine serum (Hyclone, Logan, UT). Luciferase-positive MiaPaCa-2 cells were created using the ViraPort retroviral vector, which does not require antibiotics for selection (Stratagene). After viral infection, MiaPaCa-2 cells were diluted to single cells to produce a stable luciferase-positive clone. Single colonies were screened based on luminescence signal obtained with the IVIS-100 system. The luciferase-positive Mia PaCa-2 clone was allowed to proliferate; resulting in the cells used for this study. All MIA PaCa-2 cells reported in this publication were luciferase positive, but denoted as only MIA PaCa-2. Luciferin was purchased from Xenogen, Inc. (Alameda, CA). Purified TRA-8 (mouse origin) was provided by Daiichi Sankyo (Tokyo, Japan). Gemcitabine (Eli Lilly and Company, Indianapolis, IN) was purchased from the University of Alabama at Birmingham Hospital Pharmacy. Purified mouse IgG1 K isotype control antibody was purchased from SouthernBiotech (Birmingham, AL). Fresh Tc-99m pertechnetate was purchased from Birmingham Nuclear Pharmacy (Birmingham, AL).

HYNIC conjugation and radiolabeling

A fresh 1.8 mM solution of succinimidyl 6-hydrazinonicotinate (HYNIC, courtesy Dr. Gary Bridger, AnorMED, Inc., Langley, British Columbia) in dimethylformamide was prepared. Forty picomoles was transferred to glass vials, followed by freezing at −90°C, then the solutions were vacuum dried using Advantage Benchtop Freeze Dryer (Virtis Co Inc., Gardiner, NY) with the shelf temperature at −75°C and trap at −90°C. The vials were sealed under vacuum, and kept frozen at −80°C until use. Each vial was reconstituted with 1.0 ml of sodium phosphate buffer (0.15 M, pH 7.8) containing 1 mg of TRA-8 (HYNIC:TRA-8 molar ratio = 6) (29). After a 3-hr incubation at room temperature, the mixture was transferred to Slide-A-Lyzer dialysis cassette having 10,000 MWCO (Pierce, Rockford, IL) and then immersed into the 1000 ml of PBS (pH 7.4) overnight at 4°C. The HYNIC-modified TRA-8 was labeled with Tc-99m using $SnCl_2$/tricine as the transfer ligand (30), and unbound Tc-99m was removed by G-25 Sephadex size-exclusion chromatography. The radiolabeling yield was about 60%. Protein concentrations of the collected fractions were measured by Lowry assay (31). The level of Tc-99m binding to TRA-8 was always greater than 96%, as measured by thin-layer chromatography using separate strips eluted with saturated saline and methyl ethyl ketone.

Animal preparation

Animal experiments were reviewed and approved by the Institutional Animal Care and Use Committee. Seven groups of female SCID mice (NCI-Frederick Animal Production Program, Fredrick, MD, 4~5 weeks old, n=5 for groups 1–3, 6, and 7, n=7 for group 4, n=3 for group 5) were used. The procedure for intrapancreatic tumor implantation was the following; a 1-cm incision was made in the left upper quadrant of the abdomen, and a solution of 2.5×10^6 MIA PaCa-2 cells in 40 μL of DMEM was injected into the tail of the pancreas, while the mice were anesthetized using intraperitoneal injection of xylazine and ketamine. The skin and peritoneum was closed in 1 layer with 3 interrupted 5-0 Prolene sutures. Four weeks after tumor implantation, abdominal ultrasound imaging was performed as described below, in order to select mice with matched tumor size for groups 1–5. DWI, anatomical MRI, and bioluminescence imaging were performed for groups 1–4 on days 0, 1, 2, and 3 at 4–5 weeks after tumor-cell implantation; groups 1–4 were injected with *i.v.* saline (200μl), *i.p.* gemcitabine (120mg/kg), *i.v.* TRA-8 (200μg), and *i.v.* TRA-8 (200μg) combined with *i.p.* gemcitabine (120mg/kg), respectively, on day 0 after imaging. TRA-8 and gemcitabine were injected mixed with 200μl of saline. DWI and anatomical MRI were also performed on group 5, a second

control group injected with *i.v*. saline (200μl), on days 0, 3, and 6. The mean tumor sizes of the groups 1–5 were not statistically different at the beginning of therapy. All mice in groups 1–4 were sacrificed after imaging on day 3, and histologic analysis (TUNEL staining) for tumors was followed. To assess distribution of TRA-8, animal groups 6 and 7 were *i.v*. injected with Tc-99m labeled TRA-8 (4.4MBq, 9μg) and Tc-99m labeled isotype control antibody (3.2MBq, 10μg), respectively, and single photon emission computed tomography (SPECT) and x-ray computed tomography (CT) were applied at 6 hours after injection, followed by biodistribution study at 24 hours after injection. The mean tumor weights of the groups 6 and 7 were not statistically different. All animals were anesthetized using isoflurane gas (1~2%) during imaging.

MR imaging

Small animal DWI was performed on a Bruker BioSpec 9.4T system (Bruker BioSpin Corp., Billerica, MA). The animal was placed in an animal bed equipped with circulating warm water to regulate body temperature during MRI scans. An orthogonally bent plastic board was used to prevent the transfer of the respiratory motion in chest to abdominal area, as shown in Fig. 1. DWI data were collected using a standard spin echo sequence with two *b*-factors (5 and 1000 s/mm^2) at three orthogonal gradient directions (x, y z), because no significant difference between ADC values obtained with two *b* factors and those with six *b* factors was measured in previously reported DWI study on glioma (28). The acquisition parameters are following: repetition time (TR)/echo time (TE) = 2500/32 milliseconds, diffusion separation time = 16 ms, diffusion gradient duration = 6 ms, 128×128 matrix, and a 30×30-mm field of view. A total of 3~5 1-mm thick slices (0.2-mm gap) were used to cover tumor regions of interest. Tumor was imaged using a combination of a 1H volume resonator/transmitter and a surface coil receiver (Bruker BioSpin Corp., Billerica, MA). An MR-compatible small animal respiratory gating device (SA Instrument, Inc., Stony Brook, NY) was used during the scans. A test tube filled with 70% ethanol was placed on the animal's skin adjacent to the tumor and imaged concurrently, so that ADC values in the tumor regions were adjusted using the mean ADC value of the standard in efforts to correct ADC-quantification error due to body-temperature fluctuation (32) or systemic error from the imager.

While the animal was under anesthesia, anatomical MRI to measure tumor-volume was performed using a T2-weighted spin echo sequence (RARE) with the following acquisition parameters: repetition time (TR)/echo time (TE) = 2000/48.8 milliseconds, 128×128 matrix, and a 30×30-mm field of view. Continuous 1-mm thick slices were used to cover the entire tumor region. Total acquisition time for DWI and anatomical MRI was about 35 minutes.

The tumor area was segmented from images obtained with the smaller *b* factor, based on the signal intensity between the region of interest (ROI) and background. The ADC value of each pixel of the segmented tumor region was calculated by $ADC \ln(I_1 I_2) (b_2 b_1)$, where I_1 was the intensity on the pixel with b_1 and I_2 was that with b_2. The final ADC map was obtained by averaging three ADC maps in three orthogonal directions, to acquire orientation independent ADC values. The segmentation and quantification of 70% ethanol used as the standard were implemented with the same procedure. The final ADC value of a tumor was obtained by averaging all ADC values in the whole tumor region. Tumor volume was measured by summing all voxels inside of the tumor boundary of the anatomical MR images. Segmentation of the tumor volume was performed using ImageJ, version 1.37v (National Institute of Heath, Bethesda, MD). The ADC quantification and finding best-fitting curves for ADC changes (described in result session) were implemented using computer software developed with Labview, version 8.5 (National Instruments Co., Austin, TX).

Ultrasound imaging

Ultrasound imaging was performed using a VisualSonics VEVO 660 high frequency, high-resolution ultrasound instrument with a 40 MHz probe (Toronto, Ontario, Canada). Animals were placed in the supine position for examination with B-Mode imaging (33). The largest diameter was found in the anterior-posterior plane, and this diameter as well as a transverse diameter were measured to quantify tumor area (length x width).

SPECT/CT imaging

SPECT/CT imaging was performed using a SPECT/CT dual-modality imager (X-SPECT, Gamma Medica-Ideas, Northridge, CA). In SPECT imaging, a total of 64 projections (data matrix size: 56 56 per projection) were acquired with a 50-sec acquisition time per projection, using a pinhole collimator with a 1-mm tungsten pinhole insert. The field of view was 43.8 mm, while the radius of rotation was 32 mm. Images were reconstructed using an ordered subsets expectation maximization algorithm (8 subsets and 20 iterations). The 4th-order Butterworth digital filtrations (fc=0.25, fm=0.15) provided by the vendor software were applied for all SPECT images to enhance the image quality. For the CT system, the X-ray tube was operated at a voltage of 50 kV_p and an anode current of 0.6 mA. 256 projections were acquired to obtain the CT images, and acquisition time per projection was 0.5 second. The co-registration of SPECT and CT images was performed using computer software, IDL Virtual Machine (Research System Inc, Boulder, CO). A 60-W heat lamp warmed the animal bodies, while they were under anesthesia. A consistent color scale was applied to all SPECT images, after correction for radioactive decay and dose.

Biodistribution study

Tumor, liver, and blood were collected for each animal, and those samples were weighed and the Tc-99m activity was measured using a calibrated gamma-ray counter (MINAXIγ Auto-gamma® 5000 series Gamma Counter manufactured by Packard Instrument Company, Grove, IL), decay corrected to dosing time, and converted to absolute radioactivity, and then the % of injected dose per gram of each tissue (%ID/g) was determined.

Bioluminescence imaging

Bioluminescence imaging was applied to all mice after MRI on each day using the IVIS-100 imaging system (Xenogen, Inc., Alameda, CA). Each mouse was intraperitoneally injected with luciferin at a dose of 2.5 mg (0.1 ml) and imaged after 15 minutes on a temperature controlled warm bed (37 C) with the following imaging parameters: 5–10 seconds luminescent exposure time, 8 photographic binning, 25-cm axial field of view, and 1 f-stop. Region of interest (ROI) was drawn manually around the tumor area, and the light emitted from the ROI was measured using the vendor software. Mice were imaged weekly prior to selection by bioluminescence and ultrasonography for inclusion in the therapy study. Mice with diffuse bioluminescence signal in the peritoneal cavity (leakage from implantation site, ~15% of implantations) were excluded from further study. Mice with non-spherical tumors as determined by ultrasonography were also excluded from further study.

Histologic analysis

Three tumors from each group were selected randomly after sacrificing the animals, and TUNEL staining of each tumor tissue were performed. Detailed tumor tissue staining procedure is presented in Appendix A. Two digital pictures (X250) were taken away from areas of necrosis but otherwise randomly for each tumor slice by one investigator blinded to the treatments that each animal had received, using SPOT camera on a Nikon Optiphot-2 microscope (Nikon inc., Melville, NY), interfaced with a personal computer and SPOT software. The image analysis software was ImageJ, version 1.37v (National Institute of Heath,

Bethesda, MD). The apoptotic (TUNEL) cells were segmented by the signal-intensity difference between the target cells and background in each picture, while the intensity and minimum particle-size thresholds were determined manually, and then counted in all the two pictures per tumor. The number of total tumor cells was also counted with the same procedure, and the cell density (Apoptotic cell number/total tumor cell number) was calculated. Uneven background intensity was corrected using "Rolling Ball" algorithm (34), while the radius was manually determined.

Statistical analysis

One-way analysis of variance (ANOVA) (35) was carried out using SAS® version 8.2 (SAS Institute Inc., Cary, NC) to compare the averaged ADC, bioluminescence, and tumor volume changes in mice without treatment to those treated with TRA-8, gemcitabine, and TRA-8 combined with gemcitabine. ANOVA was also applied to compare the results of TUNEL staining in tumors of mice in the four different groups.

Results

SPECT imaging and biodistribution analysis confirmed the specific uptake of Tc-99m labeled TRA-8 into orthotopic pancreatic tumor xenografts

Figure 2 shows a photograph of a representative mouse bearing an orthotopic pancreatic tumor (A), and SPECT/CT fused images (coronal view) at 6 hours after injection of Tc-99m-TRA-8 (B) or Tc-99m-isotype control antibody in another mouse (C) with the same color scaling. The dotted circle in each subfigure indicates the tumor region. There was higher tumor uptake of Tc-99m-TRA-8 as compared with the Tc-99m-isotype control antibody. From the biodistribution study, the %ID/g in tumor, liver, and blood at 24 hours after Tc-99m-TRA-8 injection was 20.0±2.2, 11.0±0.6, and 12.9±1.7 respectively, while those tissues for mice injected with Tc-99m-isotype control antibody were 9.4±1.8, 12.5±0.7, and 14.7±0.8 respectively. The tumor uptake of Tc-99m-TRA-8 was significantly ($p < 0.05$) higher than that of the Tc-99m-labeled isotype control antibody.

A significant ADC increase was detected by diffusion weighted imaging at 1 day after combined therapy or TRA-8 monotherapy

Figure 3 shows a representative set of diffusion-weighted MR images at (A) b=5 and (B) b=1000 s/mm^2 with the same gray scaling, and (C) the ADC map calculated from both the DW images. The tube filled with 70% ethanol (standard for ADC quantification) and tumor regions are indicated with dotted rectangle and circle, respectively, in Fig. 3A. Figure 4A presents the ADC changes (mean and SE) in tumors (all voxels) for groups 1–4 at 1, 2, and 3 days after treatment. The ADC value for the four groups on day 0 averaged 0.00118 0.00006 mm^2/s (mean SE, n=22). On day 1, the mean ADC changes of groups 3 and 4 were 21±9% and 27±3%, respectively, significantly ($p<0.05$) higher than that of group 1 (−1±5%) or group 2 (−2±4%). The mean ADC increases for group 4 on all the three days of measurement were higher than those of group 3, but the differences were not significant statistically ($p >0.05$). The mean ADC change of group 2 gradually increased and reached 12±9% on day 3, which was statistically different ($p<0.05$) than that of group 1. Of interest, the ADC values of group 1 (control) gradually decreased over time, which was confirmed in a repeat experiment (group 5); the mean ADC changes of group 5 (control) were −12±4% and −26±6% at 3 and 6 days after treatment respectively.

Tumor-volume and bioluminescence-signal changes for groups 1–4 are presented in Figs. 4B and 4C, respectively. Tumor-volume changes were not statistically different among any of the groups on day 1, but the mean values for groups 3 and 4 were significantly lower ($p <0.05$) than those of groups 1 and 2 on days 2 and 3. While the mean tumor volume of group 2 remained

constant, that of group 1 increased 18±14% during the 3-day monitoring period. The tumor-volume changes of group 5 (control) were 10±11% and 6±11% on days 3 and 6, respectively. Mean bioluminescence-signal changes of both the groups 1 and 2 increased about 250% during the 3 days, whereas those of groups 3 and 4 decreased 89±2% and 88±2%, respectively, during the same time period, comparable with tumor-volume decreases of groups 3 (69±5%) and 4 (74±6%).

Early ADC increase was highly correlated with apoptotic cellularity

Figure 5A shows representative photomicrographs of tumor slices (5- m thickness) following TUNEL staining. Quantifications of apoptotic cell density of groups 1–4 are represented in histograms (Fig. 5B). The apoptotic cell densities of groups 3 and 4 were significantly higher than those of the other groups, indicating the superior therapeutic efficacy of TRA-8. Figure 5C shows that the mean apoptotic cell density was linearly proportional to the mean ADC increase measured at 1 day after therapy initiation (shown in Fig. 4A).

Early ADC increase was highly correlated with survival time

Figure 6A shows the ADC changes at 1 day after treatment were linearly proportional to the mean survival time, measured in our previous study (22); the mean survival times were 76±3 (mean±SE), 79±5, 121±4, and 142±7 days, when mice were untreated (control) or treated with 2 cycles of gemcitabine, TRA-8, and TRA-8 plus gemcitabine, respectively, with the same doses used for the current study. From Fig. 6A, an equation to correlate the early ADC changes and survival times was derived as follows,

$$EST = 2.89 ADC_{1D} + 5.26 \approx 3 ADC_{1D}, \quad (1)$$

where *EST* is extended survival time (%) by treatment and ADC_{1D} is ADC change (%) at 1 day after therapy initiation. However, one major concern in the application of ADC measurement for early therapy evaluation would be that the water induced by tumor-cell killing may not be confined within the tumor boundary, but may diffuse away. As more water is generated, a higher oncotic pressure may result, causing an even faster diffusion. Therefore, the prognosis based on equation (1) might be varied according to the imaging time point after starting therapy.

A new, DWI-based imaging biomarker to measure therapeutic efficacy independently from imaging time point was proposed

Figure 4A shows that the amount of ADC increase for group 4 was decreased on each subsequent day after therapy was initiated. If the amount of extracellular water induced by apoptosis were in equilibrium with the water that was diffusing out from the tumor, then the magnitude of ADC increase relative to the baseline value would be constant. Therefore, the ADC increase over time could be modeled by

$$ADC_n = \alpha(1 - e^{-\beta n}), \quad (2)$$

where n is time (day), ADC_n is ADC change (%) relative to day 0 at n day after therapy initiation, α is the maximum ADC increase (%), and is a constant to determine the change rate of ADC increase over time. From the best-fitting curve to the ADC changes of group 4, α was estimated to be 37%. Figure 6B presents four best-fit curves for the average ADC changes in groups 1–4, when α was fixed to 37%. The β values were −0.113, 0.096, 0.634, and 1.224 for groups 1–4, respectively. Figure 6C shows that the β values were linearly proportional to the mean survival time, and therefore equation (1) can be rewritten to correlate the β values with survival times as follows,

$$EST = 69.7\beta + 5.26 \approx 70\beta. \quad (3)$$

In summary, the β value obtained from multiple DWI studies could be considered as a new imaging biomarker.

Discussion

To our knowledge, this is the first report of the application of DWI in an orthotopic pancreatic tumor model. Further, this study demonstrates the feasibility of DWI for early detection of effective therapy of an apoptosis-inducing drug for pancreatic cancer treatment. To date, DWI of orthotopic pancreatic tumor has had limited success, due to severerespiratory motion artifact in the abdominal area. To prevent motion transfer from the chest region, each tumor was secured using an orthogonally bent plastic board (Fig. 1). The pressure applied by this board was localized on the abdominal area, and did not result in respiratory difficulty or mortality of the animals. No injury or death occurred in the 98 imaging sessions, although each imaging session required approximately 1 hour including preparation time. Importantly, most DW images at even high *b* values had minor motion artifact, facilitating reproducible ADC quantification. Furthermore, high frequency ultrasound imaging was utilized to select mice bearing identical tumor sizes throughout the groups, increasing the accuracy of ADC quantification. In a previous experiment, variable tumor growth was observed in the same orthotopic pancreatic tumor model (22,36). Larger tumors may contain central necrosis (37, 38), which could increase ADC values for the tumor and be unrelated to drug-induced apoptosis.

In contrast to the significant increases of ADC values at 1 day after therapy in groups 3 and 4, tumor volumes were not changed at this same time. This confirms that extra-cellular water increase due to apoptosis preceded change in tumor size, and thereby DWI may be more sensitive than the current method (RECIST: Response Evaluation Criteria in Solid Tumors) to measure early anti-cancer efficacy following treatment. The decrease of ADC values in the control groups (2 experiments) was presumably caused by increased tumor-cell density (or fibrous tissue) over time, leading to a decrease of extra-cellular water.

Although bioluminescence imaging detected significant decrease of emitted light from tumors in groups 3 and 4 at 1 day after initiating therapy, quantification error induced by attenuation of optical light should be considered in days 2–3; that is, when tumor volume shrank, the distance from the tumor to abdominal surface became correspondingly greater, in general. Bioluminescence signal could be reduced due to contribution of signal attenuation as well as an actual decrease of viable tumor mass.

Early assessment of therapeutic efficacy is essential to prevent unnecessary treatment and optimize therapeutic strategies to extend patients' lives. ADC quantification is a safe and logical approach to establish personalized medicine and can be applied to measure effective neoadjuvant therapy. Equations 1 and 3 demonstrate how to predict the survival of animals that harbor pancreatic cancer following treatment, based on monitoring early ADC change. These equations will need adjustments following more extensive preclinical and clinical studies, in order to be used for human pancreatic-cancer prognosis, but they may serve as prototypes for future versions.

Acknowledgements

We thank Karri Folks for assistance with bioluminescence imaging, tumor dissection, and histology, and Dr. Thian Ng for valuable consultation. All experiments complied with current regulatory requirements (including ethics requirements) and laws of the United States of America.

Grant support: HSF-GEF Scholar Award, Research Initiative Pilot Award, Translational Research Pilot Project Program, AACR-Pancreatic Cancer Action Network Career Development Award, Daiichi Sankyo, NIH grants 5P50CA89019, P20CA10195, and 5P30CA013148.

References

1. Burris HA III, Moore MJ, Andersen J, et al. Improvements in survival and clinical benefit with gemcitabine as first-line therapy for patients with advanced pancreas cancer: a randomized trial. J Clin Oncol 1997;15:2403–13. [PubMed: 9196156]
2. Berlin JD, Catalano P, Thomas JP, Kugler JW, Haller DG, Benson AB III. Phase III study of gemcitabine in combination with fluorouracil versus gemcitabine alone in patients with advanced pancreatic carcinoma: Eastern Cooperative Oncology Group Trial E2297. J Clin Oncol 2002;20:3270–5. [PubMed: 12149301]
3. Rocha Lima CM, Green MR, Rotche R, et al. Irinotecan plus gemcitabine results in no survival advantage compared with gemcitabine monotherapy in patients with locally advanced or metastatic pancreatic cancer despite increased tumor response rate. J Clin Oncol 2004;22:3776–83. [PubMed: 15365074]
4. Di Costanzo F, Carlini P, Doni L, et al. Gemcitabine with or without continuous infusion 5-FU in advanced pancreatic cancer: a randomised phase II trial of the Italian oncology group for clinical research (GOIRC). Br J Cancer 2005;93:185–9. [PubMed: 15986036]
5. Louvet C, Labianca R, Hammel P, et al. Gemcitabine in combination with oxaliplatin compared with gemcitabine alone in locally advanced or metastatic pancreatic cancer: results of a GERCOR and GISCAD phase III trial. J Clin Oncol 2005;23:3509–16. [PubMed: 15908661]
6. Ibrahim SM, Ringel J, Schmidt C, et al. Pancreatic adenocarcinoma cell lines show variable susceptibility to TRAIL-mediated cell death. Pancreas 2001;23:72–9. [PubMed: 11451151]
7. Ozawa F, Friess H, Kleeff J, et al. Effects and expression of TRAIL and its apoptosis-promoting receptors in human pancreatic cancer. Cancer Lett 2001;163:71–81. [PubMed: 11163110]
8. Sheridan JP, Marsters SA, Pitti RM, et al. Control of TRAIL-induced apoptosis by a family of signaling and decoy receptors. Science 1997;277:818–21. [PubMed: 9242611]
9. Walczak H, Miller RE, Ariail K, et al. Tumoricidal activity of tumor necrosis factor-related apoptosis-inducing ligand in vivo. Nat Med 1999;5:157–63. [PubMed: 9930862]
10. Ashkenazi A, Pai RC, Fong S, et al. Safety and antitumor activity of recombinant soluble Apo2 ligand. J Clin Invest 1999;104:155–62. [PubMed: 10411544]
11. Chinnaiyan AM, Prasad U, Shankar S, et al. Combined effect of tumor necrosis factor-related apoptosis-inducing ligand and ionizing radiation in breast cancer therapy. Proc Natl Acad Sci U S A 2000;97:1754–9. [PubMed: 10677530]
12. Pan G, O'Rourke K, Chinnaiyan AM, et al. The receptor for the cytotoxic ligand TRAIL. Science 1997;276:111–3. [PubMed: 9082980]
13. Walczak H, Degli-Esposti MA, Johnson RS, et al. TRAIL-R2: a novel apoptosis-mediating receptor for TRAIL. Embo J 1997;16:5386–97. [PubMed: 9311998]
14. Chaudhary PM, Eby M, Jasmin A, Bookwalter A, Murray J, Hood L. Death receptor 5, a new member of the TNFR family, and DR4 induce FADD-dependent apoptosis and activate the NF-kappaB pathway. Immunity 1997;7:821–30. [PubMed: 9430227]
15. Schneider P, Thome M, Burns K, et al. TRAIL receptors 1 (DR4) and 2 (DR5) signal FADD-dependent apoptosis and activate NF-kappaB. Immunity 1997;7:831–6. [PubMed: 9430228]
16. Jo M, Kim TH, Seol DW, et al. Apoptosis induced in normal human hepatocytes by tumor necrosis factor-related apoptosis-inducing ligand. Nat Med 2000;6:564–7. [PubMed: 10802713]
17. Pan G, Ni J, Wei YF, Yu G, Gentz R, Dixit VM. An antagonist decoy receptor and a death domain-containing receptor for TRAIL. Science 1997;277:815–8. [PubMed: 9242610]
18. Degli-Esposti MA, Dougall WC, Smolak PJ, Waugh JY, Smith CA, Goodwin RG. The novel receptor TRAIL-R4 induces NF-kappaB and protects against TRAIL-mediated apoptosis, yet retains an incomplete death domain. Immunity 1997;7:813–20. [PubMed: 9430226]
19. Degli-Esposti MA, Smolak PJ, Walczak H, et al. Cloning and characterization of TRAIL-R3, a novel member of the emerging TRAIL receptor family. J Exp Med 1997;186:1165–70. [PubMed: 9314565]

20. Emery JG, McDonnell P, Burke MB, et al. Osteoprotegerin is a receptor for the cytotoxic ligand TRAIL. J Biol Chem 1998;273:14363–7. [PubMed: 9603945]
21. Ichikawa K, Liu W, Zhao L, et al. Tumoricidal activity of a novel anti-human DR5 monoclonal antibody without hepatocyte cytotoxicity. Nat Med 2001;7:954–60. [PubMed: 11479629]
22. Derosier LC, Vickers SM, Zinn KR, et al. TRA-8 anti-DR5 monoclonal antibody and gemcitabine induce apoptosis and inhibit radiologically validated orthotopic pancreatic tumor growth. Mol Cancer Ther 2007;6:3198–207. [PubMed: 18089714]
23. Saleh A, Srinivasula SM, Acharya S, Fishel R, Alnemri ES. Cytochrome c and dATP-mediated oligomerization of Apaf-1 is a prerequisite for procaspase-9 activation. J Biol Chem 1999;274:17941–5. [PubMed: 10364241]
24. Li P, Nijhawan D, Budihardjo I, et al. Cytochrome c and dATP-dependent formation of Apaf-1/caspase-9 complex initiates an apoptotic protease cascade. Cell 1997;91:479–89. [PubMed: 9390557]
25. Moffat BA, Chenevert TL, Meyer CR, et al. The functional diffusion map: an imaging biomarker for the early prediction of cancer treatment outcome. Neoplasia 2006;8:259–67. [PubMed: 16756718]
26. Galons JP, Altbach MI, Paine-Murrieta GD, Taylor CW, Gillies RJ. Early increases in breast tumor xenograft water mobility in response to paclitaxel therapy detected by non-invasive diffusion magnetic resonance imaging. Neoplasia 1999;1:113–7. [PubMed: 10933044]
27. Koh DM, Scurr E, Collins D, et al. Predicting response of colorectal hepatic metastasis: value of pretreatment apparent diffusion coefficients. AJR Am J Roentgenol 2007;188:1001–8. [PubMed: 17377036]
28. Chenevert TL, Stegman LD, Taylor JM, et al. Diffusion magnetic resonance imaging: an early surrogate marker of therapeutic efficacy in brain tumors. J Natl Cancer Inst 2000;92:2029–36. [PubMed: 11121466]
29. Abrams MJ, Juweid M, tenKate CI, et al. Technetium-99m-human polyclonal IgG radiolabeled via the hydrazino nicotinamide derivative for imaging focal sites of infection in rats. J Nucl Med 1990;31:2022–8. [PubMed: 2266401]
30. Larsen SK, Solomon HF, Caldwell G, Abrams MJ. [99mTc]tricine: a useful precursor complex for the radiolabeling of hydrazinonicotinate protein conjugates. Bioconjug Chem 1995;6:635–8. [PubMed: 8974465]
31. Lowry O, Rosebrough N, Farr L, Randall R. Protein measurement with the folin phenol reagent. J Biol Chem 1951;193:265–75. [PubMed: 14907713]
32. Sack I, Gedat E, Bernarding J, Buntkowsky G, Braun J. Magnetic resonance elastography and diffusion-weighted imaging of the sol/gel phase transition in agarose. J Magn Reson 2004;166:252–61. [PubMed: 14729037]
33. Pezold JC, Zinn K, Talbert MA, Desmond R, Rosenthal EL. Validation of ultrasonography to evaluate murine orthotopic oral cavity tumors. ORL J Otorhinolaryngol Relat Spec 2006;68:159–63. [PubMed: 16465070]
34. Sternberg SR. Biomedical image processing. IEEE Computer 1983;16:22–34.
35. Neter, J.; Kutner, MH.; Nachtsheim, JC.; Wasserman, W. Applied linear statistical models. 4. Columbus: The McGraw-Hill Companies, Inc.; 1996.
36. Derosier LC, Buchsbaum DJ, Oliver PG, et al. Combination Treatment with TRA-8 Anti Death Receptor 5 Antibody and CPT-11 Induces Tumor Regression in an Orthotopic Model of Pancreatic Cancer. Clin Cancer Res 2007;13:5535s–43s. [PubMed: 17875786]
37. Kim H, Chaudhuri TR, Buchsbaum DJ, Wang D, Zinn KR. Single-photon emission computed tomography imaging with a humanized, apoptosis-inducing antibody targeting human death receptor 5 in pancreas and breast tumor xenografts. Cancer biol ther 2007;6:1396–402.
38. Kim H, Chaudhuri TR, Buchsbaum DJ, Wang D, Zinn KR. High-resolution single-photon emission computed tomography and X-ray computed tomography imaging of Tc-99m-labeled anti-DR5 antibody in breast tumor xenografts. Mol Cancer Ther 2007;6:866–75. [PubMed: 17363481]

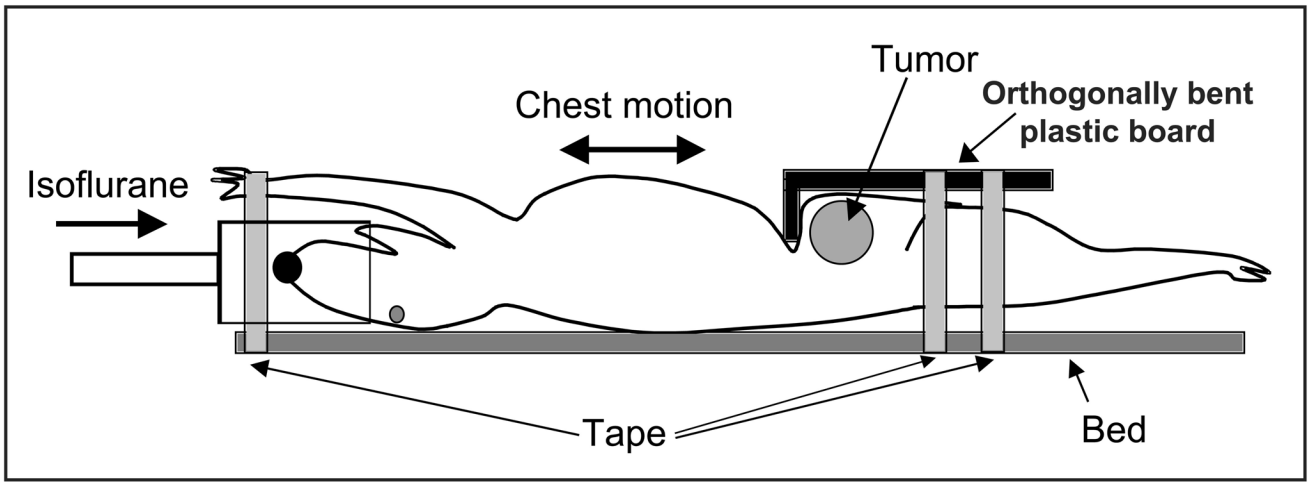

Figure 1.
Illustration for applying an orthogonally bent plastic board to minimize motion transfer from chest to abdominal area, where tumor is located.

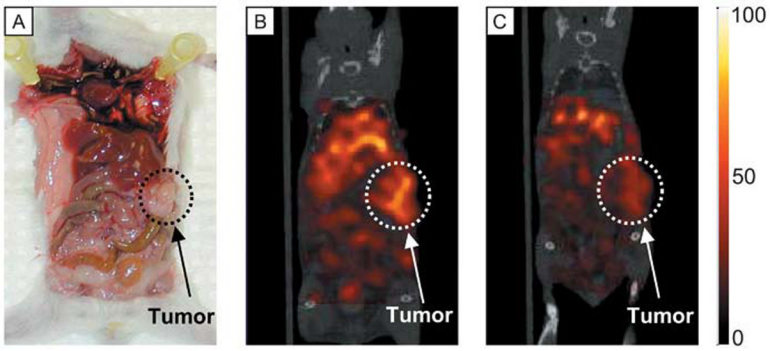

Figure 2.
(A) Photograph of a representative orthotopic pancreatic tumor, and *in vivo* SPECT/CT images (coronal view) at 6 hours after (B) Tc-99m-TRA-8 or (C) Tc-99m-isotype control antibody injection intravenously. The same color scale was applied for both the SPECT images.

Figure 3.

Representative diffusion weighted images (DWI) of a mouse bearing a MIA PaCa-2 tumor orthotopically at two different diffusion-weighting factors, (A) b = 5 s/mm^2 and (B) b = 1000 s/mm^2, with constant gray scale. (C) Apparent diffusion coefficient (ADC) map calculated from images (A) and (B). The orthotopic pancreatic tumor and a plastic tube filled with 70% ethanol (a standard for ADC quantification) are indicated with dotted circle and rectangle respectively in Fig. (A).

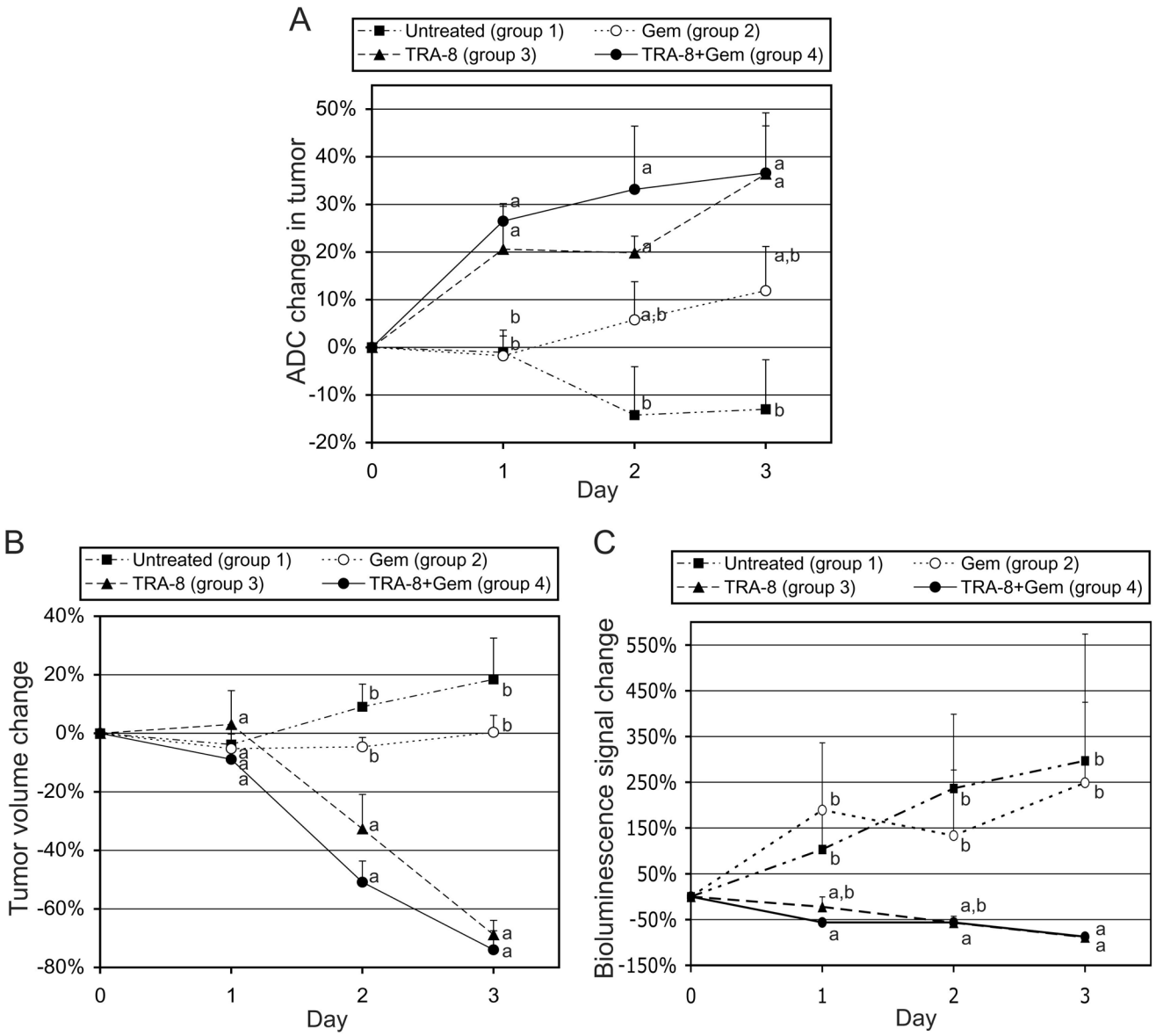

Figure 4.

Analyses of tumor response to treatment. (A) Intratumoral apparent diffusion coefficient (ADC) change, (B) tumor volume change, and (C) bioluminescence signal change, measured at 1, 2, and 3 days after initiation of therapy, when groups 1–4 were untreated and treated with gemcitabine (120 mg/kg), TRA-8 (200 μg), and combined therapy respectively on day 0. Statistical differences among groups are indicated by different letters on each day.

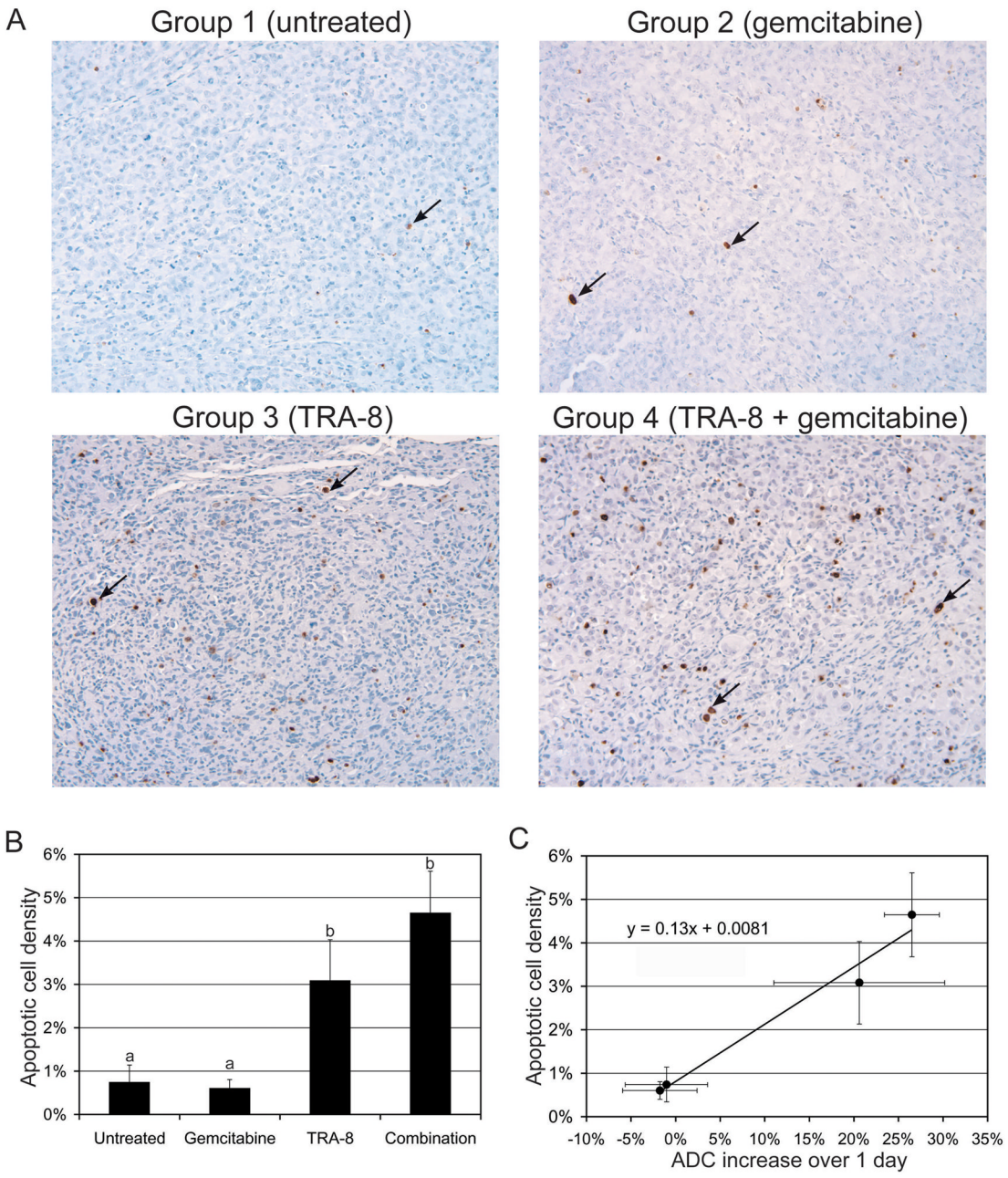

Figure 5.

Histologic analyses of tumor response. (A) Representative TUNEL (X250) staining of MIA PaCa-2 tumors collected at day 3, when saline (untreated), gemcitabine, TRA-8, and TRA-8 combined with gemcitabine were administrated respectively on day 0. An apoptotic cell is indicated with a black arrow in each sub-figure. (B) Apoptotic cell densities are presented at the four different treatments, while different letters above bars indicate statistical differences among groups. (C) Apoptotic cell density (shown in Fig. 5B) versus ADC increase over 1 day (shown in Fig. 4A).

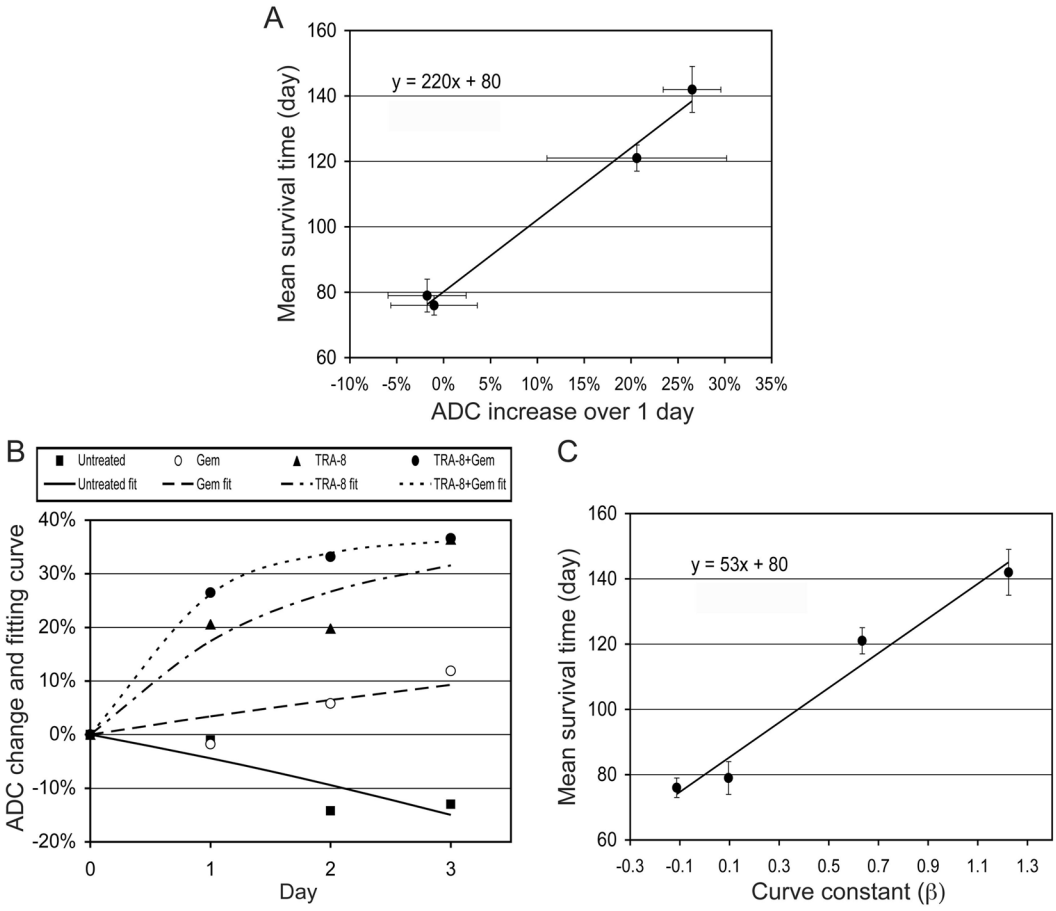

Figure 6.

Correlation between early ADC change and survival time. (A) Mean survival times (from DeRoiser et al., Mol. Cancer. Ther., 2007) versus ADC increases at 1 day after therapy (shown in Fig. 4A). The mean survival times were measured in previous experiment, when four groups (n=10 per group) of SCID mice bearing MIA PaCa-2 tumors orthotopically were untreated (control) or treated with 2 cycles consisting of multiple injections of gemcitabine, TRA-8, and TRA-8 combined with gemcitabine respectively. The dose fraction for each group was the same with that in the current study. (B) Mean ADC changes of four groups (shown in Fig. 4A) for three days after therapy initiation and best fitting non-linear curves (equation 2) with four different β values. (C) Mean survival times versus the curve constants (β).